ACS EARTH AND SPACE CHEMISTRY

Article

Cite This: ACS Earth Space Chem. 2019, 3, 2063−2075

http://pubs.acs.org/journal/aesccq

Experimental and Theoretical Studies of the Environmental Sensitivity of the Absorption Spectra and Photochemistry of Nitenpyram and Analogs

Michael J. Ezell,[†,§] Weihong Wang,[†,§] Dorit Shemesh,[‡,§] Anton Ni,[†] R. Benny Gerber,[*,†,‡] and Barbara J. Finlayson-Pitts[*,†]

[†]Department of Chemistry, University of California Irvine, Irvine, California 92697-2025, United States

[‡]Institute of Chemistry, Fritz Haber Research Center, Hebrew University of Jerusalem, Jerusalem 91904, Israel

Supporting Information

ABSTRACT: Neonicotinoid (NN) pesticides have widespread use, largely replacing other pesticides such as the carbamates. Hence, there is a need to understand their environmental fates at a molecular level in various media, especially water. We report here the studies of a nitroenamine NN, nitenpyram (NPM), in aqueous solution where the absorption cross sections in the actinic region above 290 nm are observed to dramatically decrease compared to those in nonaqueous solvents. Quantum chemical calculations show that addition of a proton to the tertiary amine nitrogen in NPM breaks the conjugation in the chromophore, shifting the absorption to shorter wavelengths, consistent with experiment. However, surprisingly, adding a proton to the secondary amine nitrogen leads to its immediate transfer to the NO_2 group, preserving the conjugation. This explains why the UV absorption of ranitidine (RAN), which has a similar chromophore but only secondary amine nitrogens, does not show a similar large blue shift in water. Photolysis quantum yields in aqueous NPM solutions were measured to be $\phi = 0.18 \pm 0.07$ at 254 nm, $(9.4 \pm 1.6) \times 10^{-2}$ with broadband radiation centered at 313 nm and $(5.2 \pm 1.1) \times 10^{-2}$ for broadband radiation centered at 350 nm (errors are 2σ). The major products in aqueous solutions are an imine that was also formed in the photolysis of the solid and a carboxylic acid derivative that is unique to the photolysis in water. Combining the larger quantum yields in water with the reduced absorption cross sections results in a calculated lifetime of NPM of only 5 min at a solar zenith angle of 35°, typical of 40°N latitude on April 1. The products do not absorb in the actinic region and hence will be long-lived with respect to photolysis.

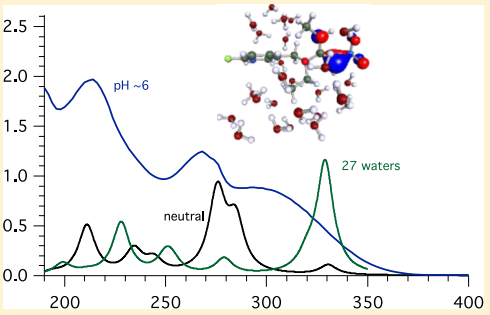

KEYWORDS: *neonicotinoids, atmospheric reactions, photochemistry, quantum yields*

INTRODUCTION

Neonicotinoid (NN) insecticides have become widely used since their introduction almost 30 years ago,[1−7] because in part of their low mammalian toxicity.[8] However, concern regarding their impacts especially on pollinators such as bees[9−26] has led to a ban on the outdoor use of the three major NN (imidacloprid, clothianidin, and thiamethoxam) in the European Union[27] and Canada.[28] These three NN are characterized by a nitroguanidine $-(N)(N)C{=}N{-}NO_2$ group. Another structural motif found in NNs is the nitroenamine group, $-(N)(N)C{=}CH{-}NO_2$, as exemplified by nitenpyram (NPM). This compound has both agricultural[1,4,6,29] as well as veterinary uses[30−34] for flea control. It is applied to a variety of crops including cotton, corn, rice, and vegetables either by spraying, coating the seeds, or applying to the soil.[29,35] As a systemic insecticide, it easily translocates throughout plant tissue, providing protection from sucking insects such as aphids. The application methods combined with rainout/washout processes result in NPM being found in agricultural products, on soil, on windblown dust particles, in aqueous environmental systems, and ultimately even in human urine.[2,4,11,12,36−42] This wide distribution makes it important to understand its chemistry and photochemistry in a number of environmental media.

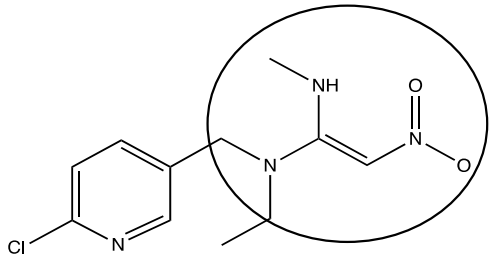

Nitenpyram

NPM absorbs light out into the actinic region beyond 290 nm that reaches the Earth's surface,[43] making photodegradation an

Received: June 20, 2019
Revised: July 31, 2019
Accepted: August 1, 2019
Published: August 16, 2019

DOI: 10.1021/acsearthspacechem.9b00179
ACS Earth Space Chem. 2019, 3, 2063−2075

important removal process in the environment. The quantum yields for photolysis of solid NPM as might be characteristic of NPM on soils or dust were measured[44] to be 9.4×10^{-4} for broadband radiation centered at 350 nm, 1.0×10^{-3} at 313 nm, and 1.2×10^{-2} at 254 nm, resulting in an atmospheric lifetime of 36 min at a solar zenith angle of 35°. However, in water, the intensity of the strong absorption band around 350 nm was observed to decrease dramatically,[44] which has important implications for photodegradation in lakes, rivers, streams, and ponds, and highlights the sensitivity of environmental processes and lifetimes to the media in which the molecule is found. Two recent studies[45,46] reported quantum yields of NPM photolysis in water that were significantly larger than for the solid.

The goals of the present study were to elucidate the mechanistic basis for the change in the absorption spectrum of NPM in water compared to other solvents such as acetonitrile (ACN) through a combination of theory and experiment and to assess the implications for the effects of the matrix on the environmental lifetime and fate of NPM. We report here experimental measurements of UV−vis and infrared absorption spectra of NPM in water as a function of pH and the quantum yields and products for photolysis at pH ∼ 6. To explore if the observations are more generally characteristic of the nitroenamine group, changes in the UV−vis spectra of ranitidine (RAN), which also contains this functionality, were carried out.

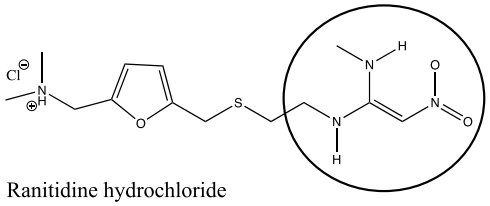

Ranitidine hydrochloride

Ranitidine hydrochloride is the active component in widely used medications to treat acid reflux and gastric ulcers, and hence a number of studies of the structure and reactivity of RAN analogs have been reported.[47−55] For example, previous calculations for some small nitroenamines assigned the 330 nm band in a neutral species to a transfer of electron density from the enamine group (C═C−N−) to the $-NO_2$ group.[56,57] Dumanovic et al.[51] calculated absorption spectra for $(CH_3NH)_2C{=}CHNO_2$ and its protonated forms, showing that there would be no significant light absorption above ∼230 nm in water for the C-protonated species. Dhaked and Bharatam[55] carried out quantum chemical calculations on different structures of *N*-ethyl-*N*-methyl-2-nitro-1,1-ethenediamine and also considered the effects of solvation by up to four water molecules. They predicted that the enamine form, $(R_1N)(R_2N)C{=}CH{-}NO_2$, was the most stable form of the neutral microsolvated molecule. They suggested that in acidic aqueous media, the protonation on carbon dominates, although protonation on the $-NO_2$ group can also contribute significantly.

To the best of our knowledge, the calculations carried out in this work are the first so far to predict the absorption spectrum of NPM itself and its protonated forms and to provide a comprehensive, molecular-level interpretation of all parts of the spectrum. Surprising differences in the effect of water on the absorption spectra of NPM compared to RAN are consistent with the quantum chemical calculations on NPM and reveal a unique proton transfer process not previously reported.

EXPERIMENTAL SECTION

Infrared Spectra. The NPM absorption spectra of solutions were obtained by Fourier transform infrared spectroscopy (Mattson RS). To avoid interference from the strong absorption of the bending mode of water in the 1600 cm^{-1} region, NPM was dissolved in D_2O (Acros 99.8% or Cambridge Isotope 99.9%) at concentrations of ∼0.15 M, which has a typical pH of ∼6. Spectra of aqueous thin films sandwiched between ZnSe windows were obtained as a function of pH in the range of 6−1, adjusted by adding solid $NaHSO_4{\cdot}H_2O$ (Fisher Chemical, Certified Grade), where pH paper (pHdrion and/or pHast) was used to determine the approximate pH. In one case, the most acidic solution (pH ∼ 1) was partially neutralized by the addition of NaOH (Fisher, 98.8%). Solutions of ranitidine hydrochloride (Sigma ≥98%) in water or D_2O at a concentration of ∼0.1 M were prepared, and the spectra measured as a function of pH as described for NPM. Experiments were not carried out at pH > 6 because NPM is known to hydrolyze under basic conditions,[45] consistent with irreversibility in the infrared spectra when the pH was increased to ∼10 and then made acidic some days later.

UV−Visible Absorption Spectra. Solutions described above were diluted by the addition of either water or D_2O to obtain the UV−vis absorption spectra of NPM (or RAN) at typical concentrations of 1.5−3.5 mM in a quartz cell of pathlength 1.0 mm with a HP 8452A photodiode array spectrometer. For comparison, spectra were also acquired in ACN at concentrations from ∼1 to 3 mM.

Actinometry and Quantum Yields. Photolysis was performed using three different lamps: (1) a low-pressure mercury lamp at 254 nm (Jelight, 81-3306-2, ozone free); (2) an organic phosphor-coated low-pressure mercury lamp with broadband emission from 290 to 350 nm and centered at 313 nm (Jelight, 84-2061-2); and (3) an organic phosphor-coated low-pressure mercury lamp with broadband emission from 310 to 425 nm and centered at 350 nm (UVP, D-28865). The lamp was covered and placed at a fixed distance from a quartz cuvette (1 cm pathlength, 4 mL volume, Starna Cells, 3-Q-10) containing the solution. The lamp was stabilized for 30 min before the photolysis experiments. To expose the cuvette to UV light, the cover was lifted to avoid turning the lamp off between each photolysis interval. For photolysis at 313 and 350 nm, a pyrex glass filter was used to remove wavelengths below 290 nm. Figure S1 in the Supporting Information (SI-I) shows the emission spectra of the lamps and the transmission of the glass filter.

In order to calculate the quantum yield of NPM, *o*-nitrobenzaldehyde (ONB) whose quantum yield in solution is established as 0.41 was used as an actinometer.[58] Samples of ONB were dissolved in ACN in concentrations from 0.1 to 0.25 mM. UV−vis spectrometry provided fast, in-situ measurements during photolysis. The absorbance at 250 nm was used to follow the loss of ONB from which the photolysis rate constant (k_{ONB}) was obtained from the first-order decay of ONB. Details of the k_{ONB} measurements and their conversion to absolute light intensities are presented in SI-II.

To identify photolysis products, NPM was dissolved in water at initial concentrations of $\sim 10^{-6}$ M and sampled as a function of photolysis time. After each photolysis interval, 60 μL of solution was withdrawn for analysis using UPLC−ESI−MS/MS (Waters, Quattro Premier XE). NPM was quantified using the multiple reaction monitoring method in positive ion mode

DOI: 10.1021/acsearthspacechem.9b00179
ACS Earth Space Chem. 2019, 3, 2063−2075

following the transition of m/z 271 to m/z 225. Identification of the photolysis products was performed using an HPLC coupled to a single quadrupole mass spectrometer and photodiode array detector (Waters, Acquity, H QDa). The mass spectrometer was operated in positive ion mode and scanned from m/z 100 to 600 and the PDA was scanned from 220 to 500 nm. A triple quadrupole mass spectrometer equipped with an ESI ionization source (Waters, Xevo TQ-S) was also used to identify the products. An aqueous solution of NPM photolysis products was injected directly into the ESI−MS source in infusion mode (no chromatography). The TQ-S was operated in positive ion mode for both full scan MS and product ion scan modes. Details of the analytical parameters can be found in SI-III.

QUANTUM CHEMICAL CALCULATIONS

NPM is known to exist in two isomeric forms, which differ by the relative orientation of the secondary −NH and $-NO_2$ group. The *E* form has an intramolecular hydrogen bond between an oxygen and the −NH group, which is seen in the crystal structure;[59] however, the *Z*-form cannot form a comparable hydrogen bond to the tertiary amine nitrogen. Different structural conformers for each form have not been reported in the literature. Therefore, a systematic conformational search was carried out starting with a single molecule in the *E* form. The potential energy surface used was PM3 using the Spartan program.[60] Twenty lowest conformers were chosen for further refinement. From these structures, the *Z* conformers were created by rotating the NO_2 group around the double bond. All these conformers were optimized using the OM2 potential[61] implemented in the MNDO[62] program.

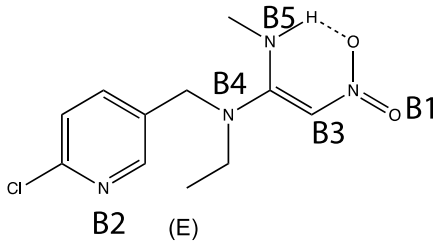

(E)

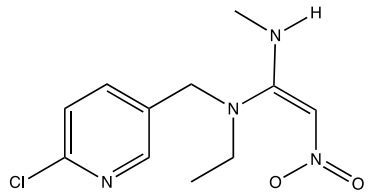

(Z)

Because semiempirical methods such as PM3 and OM2 lack the parameterization for the chlorine atom, fluorine was substituted for chlorine. This was done also in our previous work on photochemistry of imidacloprid[63] where it was shown that the excitation energies are not significantly affected by the substitution. While the substitution of Cl by F in our model is an approximation and in some other circumstances can give rise to problems, this substitution can be readily justified in the present case. The difficulties in replacing Cl by F in photochemical calculations arise when the halogen is significantly involved in the excitation. Analysis of the atomic orbitals participating in the total electronic wavefunction indicates that the halogen orbitals are involved very little in the excitation. In this respect, this system is similar to IMD so that the validation in a previous study[63] of the substitution of Cl by F in the case of IMD should also apply for NPM.

The lowest 8 *E* conformers and 8 *Z* conformers were further optimized at the singlet ground state with MP2 in conjunction with the resolution-of-the-identity approximation[64] for the evaluation of the electron-repulsion integrals implemented in Turbomole.[65] The cc-pVDZ basis set has been successfully employed.[66] Boltzmann distributions were calculated for each conformer at a temperature of 300 K. Ten vertical excitation energies were calculated for the lowest conformer using ADC(2) implemented[67] in Turbomole. ADC(2) has been used in previous studies and has been proven to be accurate for spectrum calculations and for photochemical reaction dynamics of organic systems.[68−71] Additionally, in order to test the effect of solvation on the absorption spectrum, the lowest E conformer structure was microsolvated by 27 water molecules, optimized by OM2 and followed by MP2/cc-pVDZ, and ten vertical excitation energies were calculated by ADC(2). Furthermore, ground-state dynamics of NPM microsolvated by 27 water molecules were run on the OM2 potential energy surface.

Calculations were carried out for a number of different protonation sites in order to simulate the full spectrum over a range of acidic pH. Five protonation sites marked **B1**−**B5** on the structure shown above were considered for contribution to the spectrum: (1) the oxygen of the $-NO_2$ group (**B1**), (2) the nitrogen in the pyridine ring (**B2**), (3) the sp^2 carbon atom (**B3**) (as suggested by Cholerton et al.),[47] (4) the tertiary nitrogen (**B4**), and (5) the secondary nitrogen (**B5**). For all protonated molecules, ten vertical excitation energies were computed using ADC(2). For all calculated sets of vertical excitation energies (for the neutral as well as for the protonated forms), a Lorentzian with a gamma of 5 nm was added in order to induce broadening of the spectrum. A composite spectrum was formed by adjusting weights of each species such that the best fit to the experimental spectrum was obtained either visually or by nonlinear optimization using the generalized reduced gradient method (Excel Solver; see SI-IV). In the latter case, the square of the relative differences between an experimental spectrum (pH ∼ 1 or pH ∼ 6) and the proposed composite spectrum was calculated at each of 21 fixed wavelengths spaced between 200 and 350 nm. The objective of Solver was to minimize the square root of the sum of these squared differences by varying the contributing weights of calculated spectra appropriate to each experimental pH.

RESULTS AND DISCUSSION

UV−Visible Absorption Spectra. The UV−vis spectra of NPM in water as a function of pH are shown in Figure 1. Also shown for comparison is the spectrum in ACN. At pH ∼ 1, there is no significant absorption above 290 nm. Even in water at pH ∼ 6, there is a dramatic decrease in the absorption beyond 300 nm compared to the ACN spectrum as reported earlier, and the change is reversible.[44] That is, if NPM is dissolved in ACN, the solvent is evaporated, and then water is added, the spectrum is the same as if NPM had been directly dissolved in water. The same is true if NPM was first dissolved in water and the water is evaporated and then dissolved in ACN.

Quantum chemical calculations were carried out on both the *E* and *Z* forms of NPM shown above. The *E* form with hydrogen-bonding between the $-NO_2$ group and the amine N−H group was the most stable structure. Absorption spectra were then calculated for this stable *E* form as well as structures to which a proton was added (Figure 2a−f). Note that quantitative

DOI: 10.1021/acsearthspacechem.9b00179
ACS Earth Space Chem. 2019, 3, 2063−2075

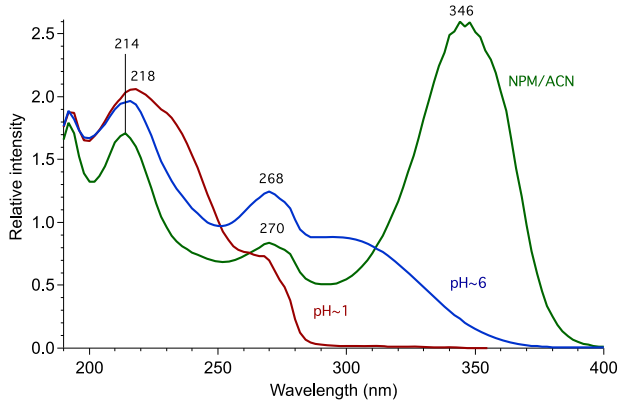

Figure 1. UV−vis absorption spectra of 0.94 mM NPM in ACN and of 1.5 mM in water at pH ∼ 6 and ∼1.

agreement between predicted and measured spectra is not expected because the calculations are for isolated molecules, rather than in aqueous solution.

Figure 2a shows the predicted spectrum (black) for a neutral, isolated molecule of NPM, and for comparison, the spectrum (blue) in water at pH ∼ 6. The structure of enamines (C═C−N) is such that the lone pair on the amine nitrogen can be delocalized into the π alkene system if the C═C is coplanar with the nitrogen and its two substituents. This results in a conjugated system with absorption at longer wavelengths than for an isolated C═C group.[72,73] For vinyl amines with an $-NO_2$ group on the β-carbon (**B3**) or a second amine group on the α-carbon (characteristic of both NPM and RAN), the degree of planarity is very high, from 84 to 100%,[72] indicating strong conjugation and delocalization to include the two amines and the $-NO_2$ group. Both NPM and RAN have these features in common and are therefore expected to be relatively planar and have similar absorption spectra.

The calculations predict that in neutral isolated NPM, the lowest energy transition at 330 nm is due to an n → π^* transition that involves a non-bonding electron on an $-NO_2$ oxygen being excited to π^* on the C═C and the $-NO_2$ group, with some involvement of the amine nitrogens. Figure 3a shows the highest

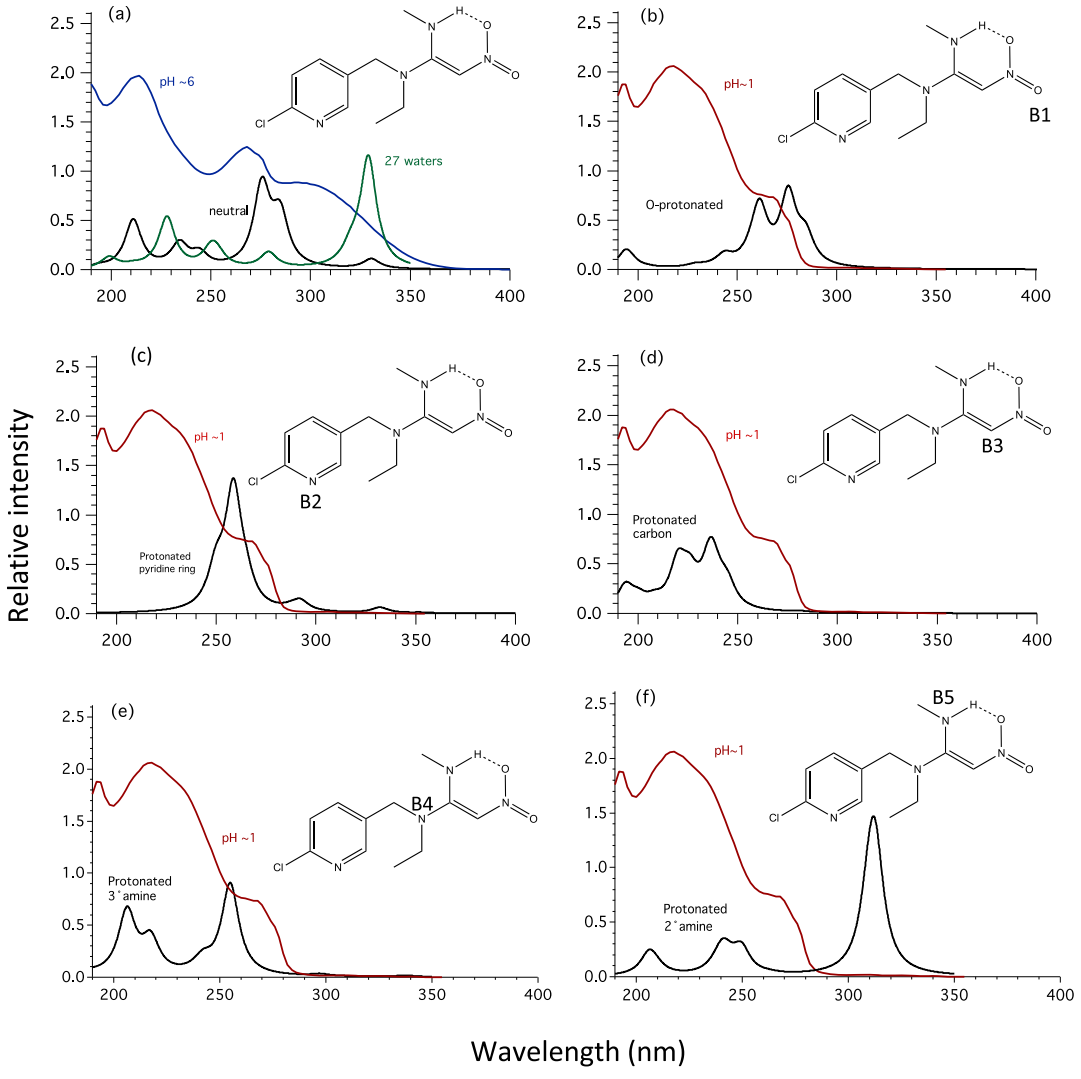

Figure 2. Predicted spectra for NPM as (a) neutral molecule (black) and as neutral NPM with 27 waters (green); and protonated at (b) oxygen of the $-NO_2$ group (**B1**); (c) pyridine ring (**B2**); (d) carbon in the enamine (**B3**); (e) tertiary nitrogen in the enamine group (**B4**); and (f) secondary nitrogen in the enamine group (**B5**). Note in the latter case that the proton actually transfers to the $-NO_2$ group; see text and Figure 3c. Also shown for comparison are the experimentally measured spectra at pH ∼ 6 (blue, part a), and ∼ 1 (red, parts b−f).

DOI: 10.1021/acsearthspacechem.9b00179
ACS Earth Space Chem. 2019, 3, 2063−2075

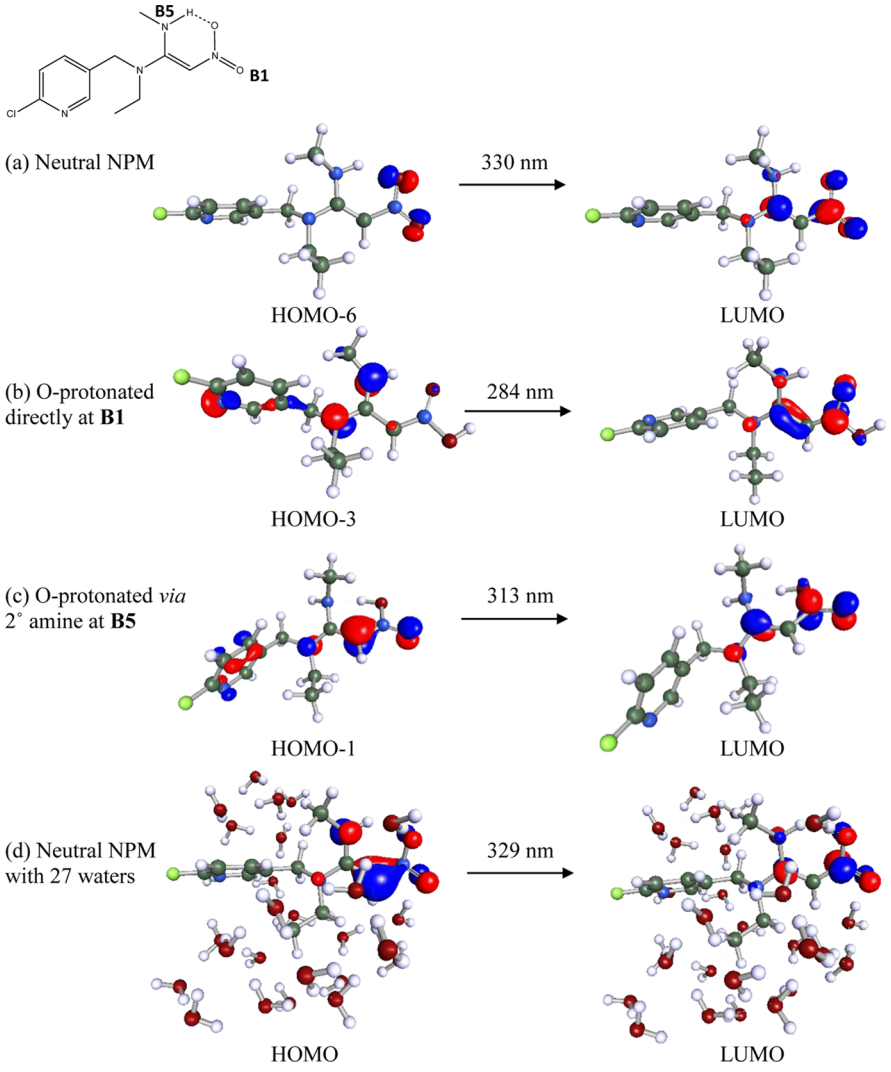

Figure 3. HOMOs and LUMO predicted for the primary, lowest energy transitions in (a) neutral NPM; (b) NPM protonated by adding a proton directly to the non-hydrogen-bonded oxygen of the $-NO_2$ group (**B1**); (c) NPM to which a proton has been added initially to the secondary amine nitrogen (**B5**) and has then transferred to the other oxygen of the $-NO_2$; and (d) neutral NPM that is solvated by 27 water molecules.

occupied molecular orbital (HOMO) and lowest unoccupied molecular orbital (LUMO) primarily involved in this transition and the associated wavelength (predicted higher energy transitions are shown in SI-V).

Figure 2b shows the spectrum predicted for protonation at the oxygen of the $-NO_2$ group (**B1**). In this case, the absorption above 300 nm is lost and the lowest energy transition is at 284 nm. This transition is from π orbitals located on the secondary and tertiary nitrogens to the π^* orbitals on $-NO_2$ and C═C, as seen in the HOMO and LUMO in Figure 3b. We refer to this species as "O-protonated" in the following discussion.

Protonation at the nitrogen of the pyridine ring (**B2**) is another possibility for which the predicted spectrum is shown in Figure 2c. The calculations predict absorption remains at 332 nm, which is not surprising because the pyridine ring is separated from the chromophore responsible for the 332 nm peak. While the pK_a associated with protonation of this site in NPM is not known, those of a number of substituted pyridines have been reported.[74] The pK_a for 2-fluoropyridine, the small molecule analog for which the calculations were performed, is −0.44, and that for 2-chloropyridine, the analog for NPM, is 0.72.[74] These values suggest that NPM will only be protonated on the pyridine ring in highly acidic solutions.

Protonation sites **B3**−**B5** are part of the enamine structure where conjugation between the C═C and lone pairs on the nitrogens in the neutral molecule leads to absorption beyond 300 nm. Protonation of either nitrogen or carbon is possible.[73,75] In NPM, there are two amine nitrogens as part of the enamine system, one a secondary and one a tertiary nitrogen. For both primary and secondary enamines, protonation of the nitrogen is generally thought to be dominant due to the kinetics, but thermodynamics favors protonation at the β-carbon.[72,73] Figure 2d shows the spectrum predicted for protonation at the carbon (**B3**). Again, there is no absorption above 300 nm. As discussed below, the pK_a associated with protonation of the alkene carbon in a different nitroenamine, RAN, was reported to be 2.19.[51] Thus, the protonated carbon species would be expected to contribute to the spectrum only under very acidic conditions.

However, for tertiary enamines such as *N*,*N*-dimethylvinylamine and 1-(dimethylamino)isobutene, protonation occurs at the nitrogen in a manner analogous to saturated amines.[72,73] The pK_a for the tertiary nitrogen in NPM has not been reported but that for 1-(dimethylamino)isobutene has been measured[72]

DOI: 10.1021/acsearthspacechem.9b00179
ACS Earth Space Chem. 2019, 3, 2063−2075

as 7.85. Thus, the tertiary nitrogen in NPM would be expected to protonate at neutral to mildly basic pH, as is the case for aliphatic amines.[74] Figure 2e shows the spectrum predicted for protonation at the tertiary (**B4**) nitrogen; absorption no longer occurs above 300 nm, as expected for disruption of the planarity and conjugation of the enamine group.

Finally, protonation can occur at the secondary nitrogen (**B5**). Calculations were initiated for a proton attached to this nitrogen, but during optimization of the structure, the proton shifted to the oxygen of $-NO_2$. In this case, there is a strong absorption at 313 nm as shown in Figure 2f, in contrast to Figure 2b where there is no significant absorption above 290 nm. Note the differences in structures resulting when a proton was added directly (Figure 3b) to the oxygen of NO_2 compared to when it was added indirectly from the protonated secondary amine (Figure 3c). Figure 3c shows the HOMO and LUMO for the major transition involved in the 313 nm absorption predicted for initial protonation at **B5**. We refer to this species as "O-protonated secondary amine" to distinguish it from **B1**.

It is perhaps initially surprising that the two different protonation scenarios (**B1** and **B5**) on the $-NO_2$ group give such different absorption spectra. However, as seen in Figure 3b,c, both the HOMO and the LUMO are quite different for these two cases. For the O-protonated form (Figure 3b), there is significant electron density on the amine nitrogens in the HOMO and on the C═C and $-NO_2$ in the LUMO. For the O-protonated secondary amine where the proton was transferred from the secondary nitrogen (Figure 3c), there is less electron density in the HOMO on the secondary amine, which is still interacting with the transferred proton.

The effects of water on neutral NPM were investigated by calculating the spectra for a single water molecule associated with the $-NO_2$ group or with the tertiary nitrogen. The effects on the spectra were relatively small compared to the effects of protonation and did not significantly impact the absorption above 300 nm. Calculations were also performed for 27 water molecules with one NPM. Figure 2a (green) shows that this solvated NPM has a strong absorption at 329 nm due to a transition from π on C═C and the secondary amine to π^* on $-NO_2$ (see Figure 3d and SI-V, VI for HOMO and LUMO and for the solvation dynamics). Water clearly enhances the absorption above 300 nm. However, this is in opposition to the decreased light absorption in water that is experimentally observed (Figure 1), establishing that solvation of NPM is not responsible for the reduction above 300 nm from ACN to water. It is noteworthy that the predicted spectrum for solvation by water is similar to that by ACN (Figure 1) and other solvents,[44] suggesting that these solvents likely interact with NPM in a similar manner. The studies of the effects of hydration on neutral NPM show that first, there are no major structural changes in the system due to hydration, and second, that the presence of water itself does not predict a reduction of intensities as observed in the experiment.

Clearly, none of the individual spectra capture all of the major features of the experimental spectra, suggesting that they contain contributions from more than one structure. As an example, Figure 4 shows the predicted spectrum for a linear combination of these structures. Figure 4a shows the composite spectrum for 56% protonation at the carbon (**B3**), 12% at the $-NO_2$ group (**B1**), and 32% at the tertiary nitrogen (**B4**) as might be expected in highly acidic media. It is emphasized that these weights are chosen to see if the shifts in the absorption spectra predicted theoretically are qualitatively consistent with the experimentally

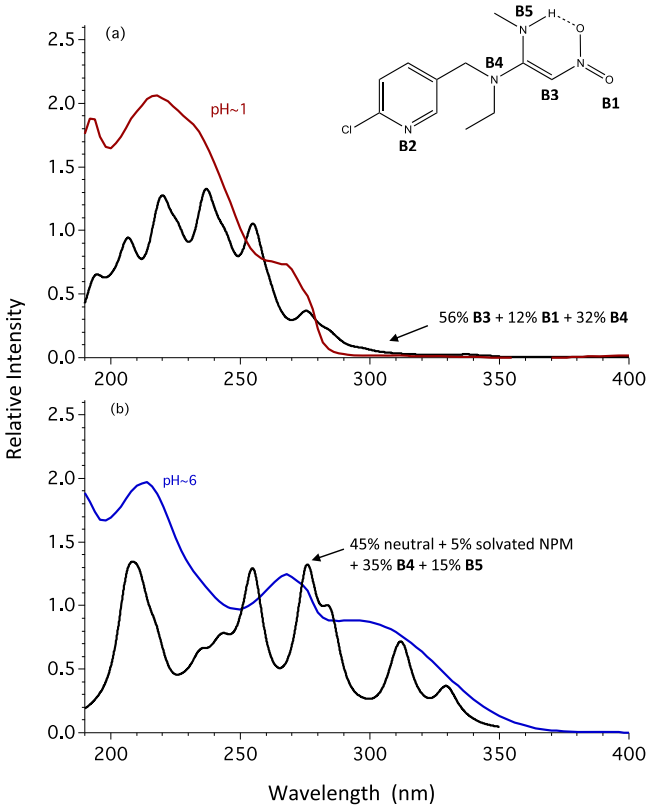

Figure 4. Composite spectra predicted for NPM using (a) combination of 56% protonation at the carbon (**B3**), 12% at the $-NO_2$ group oxygen (**B1**), and 32% at the tertiary nitrogen (**B4**) compared to the experimental spectrum at pH ≈ 1; (b) combination of 45% neutral NPM, 5% NPM with 27 H_2O, 15% protonation at the secondary nitrogen (**B5**), and 35% protonation at the tertiary nitrogen (**B4**), compared to the experimental spectrum at pH ~ 6.

observed effects of pH. While the choice is somewhat arbitrary, it gives a reasonable fit to the experimental spectrum. The comparison provides molecular-level insight and suggests that NPM exists as a mixture of species that are protonated at different sites. At pH ~ 6, light absorption above 300 nm has changed significantly from that in ACN (Figure 1), although is it not completely suppressed as under very acidic conditions. This suggests that some protonation that breaks the conjugation in the enamine system is already occurring under slightly acidic conditions, which is reasonable given that protonation of the tertiary nitrogen (**B4**) is expected. Figure 4b shows the composite spectrum from 45% neutral NPM, 5% from solvated NPM where there is significant absorption at 329 nm, 35% at the tertiary nitrogen (**B4**), and 15% from the O-protonated secondary amine structure (**B5**). The composite spectrum captures the major features and the wider absorption range, especially above 300 nm.

In short, these first calculations on NPM illustrate the importance of protonation at different sites in the molecule, which are very sensitive to pH, and how this impacts the absorption spectra (and ultimately lifetimes in the environment, see below). They also show how water can affect the transitions and that a combination of these transitions can produce composite spectra that are reasonably consistent with the experimental measurements.

To provide further insight into the effect of solvent and pH on the absorption spectra, similar experiments were carried out on

DOI: 10.1021/acsearthspacechem.9b00179
ACS Earth Space Chem. 2019, 3, 2063−2075

RAN. This molecule is structurally similar to NPM in that it has a nitroenamine group that contributes to strong light absorption beyond 300 nm. It also exists in two isomeric forms, *E* and *Z*, but has two secondary amines rather than one secondary and one tertiary:

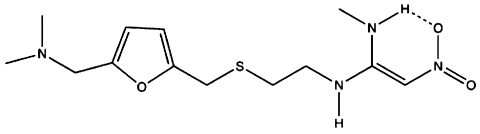

(E)

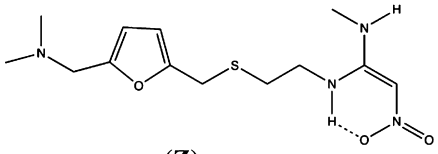

(Z)

Figure 5 shows the RAN spectra in ACN, in water at pH ∼ 6 and at pH ∼ 1. Light absorption above 300 nm is dramatically

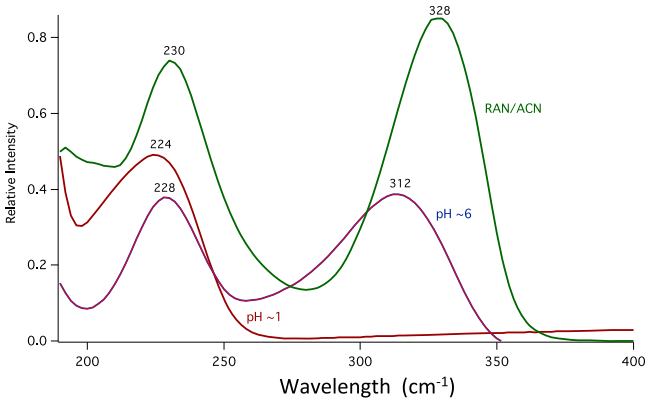

Figure 5. UV−vis absorption spectra of 3.0 mM RAN in ACN and 3.5 mM in water at pH ∼ 6 and ∼1. The spectrum in ACN has been scaled by 0.35 for direct comparison to the spectra in water.

decreased in highly acidic media similar to NPM, which is in agreement with earlier work on RAN.[47,51] This was attributed to loss of conjugation due to protonation of the alkene carbon:[51]

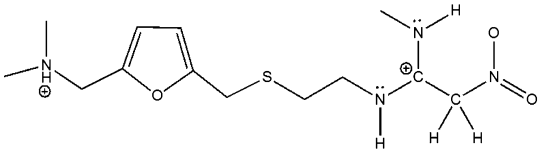

Thus, C-protonation in RAN should play a role under highly acidic conditions (pK_a 2.19),[51] consistent with the predictions for NPM at **B3**. Note that the pK_a of the tertiary nitrogen in the terminal dimethylamine group in RAN has been measured to be 8.1,[51] so it too will be protonated, but because it is far removed from the chromophore, it will not impact the spectrum.

However, unlike NPM, mildly acidic aqueous solutions do not have a dramatic effect on the peak position spectrum compared to ACN (Figure 5), although it does reduce its intensity. One difference between NPM and RAN in the vicinity of the enamine group is that NPM has one secondary and one tertiary amine attached to the alkene carbon, whereas RAN has two secondary amines. As discussed above, tertiary nitrogens in enamines behave like aliphatic amines and will be protonated under mildly basic to acidic solutions,[72,73] breaking the conjugation responsible for light absorption above 300 nm. However, adding a proton to the secondary nitrogen in NPM results in transfer of the proton to the $-NO_2$ group (Figure 3c), which does not break the conjugation or reduce the light absorption above 300 nm (Figure 2f). Assuming the same is true for RAN, only in highly acidic solutions is the conjugation in the enamine group in RAN broken due to protonation at the carbon. In mildly acidic solutions, protonation of either secondary amine should result in transfer to the $-NO_2$, preserving light absorption above 300 nm. Another pharmaceutical, nizatidine, which has a very similar structure to that of RAN with two secondary amine nitrogens, shows the same behavior as RAN in ACN and water, that is, it also does not show the dramatic shift in the peak for its absorption in water that is seen with NPM.

Infrared Spectra. Figure 6 shows the transmission infrared spectra of NPM in D_2O at pH ∼ 6 and pH ∼ 1 in the 1700−1300

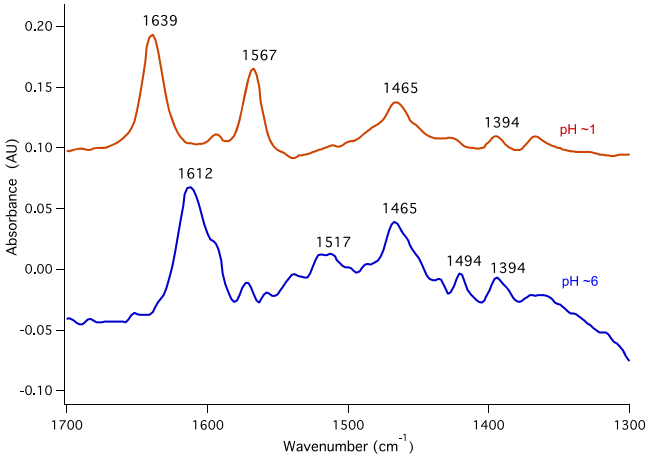

Figure 6. Infrared spectra of 0.15 M NPM in D_2O at pH ∼ 6 and ∼1.

cm^{-1} region (D_2O has a broad and strong absorption band around 1200 cm^{-1} that makes seeing peaks in this region difficult). At near neutral pH, peaks at 1612, 1517, and 1465 cm^{-1} are seen. Figure 7 shows analogous spectra for RAN, where significant absorption bands are observed at 1602, 1515, and 1456 cm^{-1}. The spectrum of a highly acidified solution that was then restored to pH ∼ 5 using NaOH showed the same peaks as the original pH ∼ 5 spectrum, suggesting that the changes were reversible. Based on known functional group assignments,[76] the

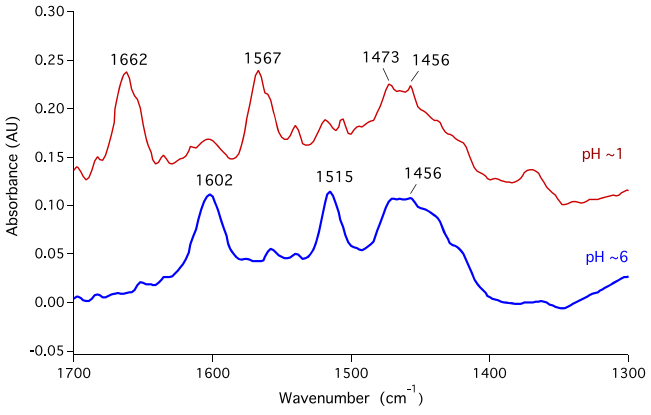

Figure 7. Infrared spectra of 0.11 M RAN·HCl in D_2O at pH ∼ 6 and ∼1 (blue).

DOI: 10.1021/acsearthspacechem.9b00179
ACS Earth Space Chem. 2019, 3, 2063−2075

1612 and 1602 cm^{-1} bands in NPM and RAN, respectively, are assigned to a protonated amine group. The pK_a values for tertiary amines are typically in the 8−10 range;[74] the pK_a for the terminal tertiary amine in RAN has been reported to be 8.13.[51] Thus, under neutral to mildly acidic conditions, the tertiary nitrogen in NPM and the terminal tertiary amine in RAN should be protonated. There may also be a contribution in this region from the C═C stretch.[72] The peaks at 1515−1517 cm^{-1} are assigned to the asymmetric $-NO_2$ stretch[76] in neutral NPM and in NPM which has a proton transferred to the $-NO_2$ group from protonation at the secondary nitrogen (Figure 3c). A number of groups absorb in the 1465 cm^{-1} region, including asymmetric $-CH_3$ bending, $-CH_2-$ scissoring vibrations, and ring stretching vibrations in the pyridine ring.[76]

As seen in Figures 6 and 7, under highly acidic conditions, the major peaks in the 1500−1600 cm^{-1} region are blue-shifted. The formation of the carbon-protonated species (**B3**) has resonance structures that involve protonated amidines (N−C═NH^+R):

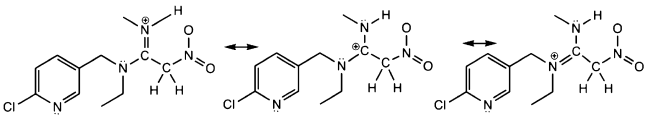

Amidines have very strong absorptions in the 1580−1685 cm^{-1} region,[76] and the 1639 and 1662 cm^{-1} peaks are assigned to this group for acidified NPM and RAN, respectively. The UV−vis spectra suggest that there is also a significant contribution from an O-protonated species (**B1**) (Figure 3b) in acidic solutions (Figure 4a). Hence, there may also be a contribution to this band from −C═N in the $-NO_2$ protonated species and its resonance structures:

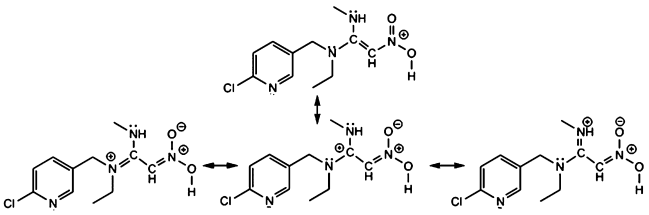

The 1567 cm^{-1} peaks for both NPM and RAN are assigned to the asymmetric $-NO_2$ stretch which is shifted in the cation compared to the 1515−1517 cm^{-1} peaks at pH ∼ 6. Stretching frequencies of isolated functional groups such as CH═O and C═N are typically at higher wavenumbers compared to situations where there is α,β conjugation.[76] Formation of the cation removes the conjugation and hence the $-NO_2$ absorption would be expected to blue-shift, as is observed (Figures 6 and 7).

Photochemistry and Quantum Yields of NPM in Water. The decay of NPM in water was followed using UPLC−MS as a function of photolysis time using the three lamps described earlier.[44] Figure 8 shows typical decays for each wavelength. The loss of NPM was first order in all cases, and the photolysis rate constants k_p (s^{-1}) are shown in Table 1. Using the measured absorption cross sections as a function of wavelength, the quantum yields were calculated using eq 1

$$k_p = \phi \sum_{\lambda} I_\lambda \sigma_\lambda \quad (1)$$

where ϕ is the photolysis quantum yield, defined as the number of molecules reacted per photon absorbed, σ_λ is the absorption cross section (base e), and I_λ is the absolute light intensity incident on the sample in photons cm^{-2} s^{-1}. This intensity was obtained as a function of wavelength from the relative lamp intensities and measurements of total light intensity using ONB as an actinometer (SI-1I). Quantum yields obtained in this fashion are averages over the wavelength range covered by each lamp.

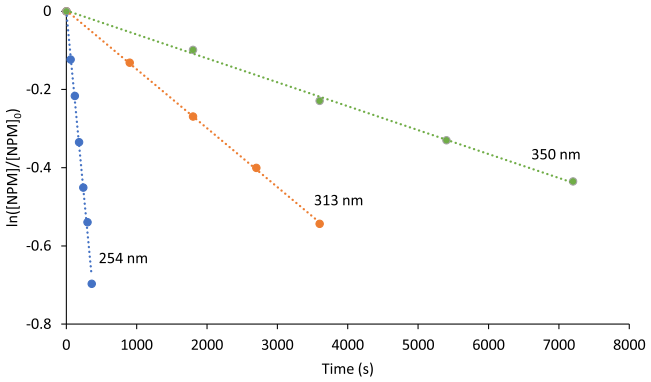

Figure 8. Typical first-order decays of NPM in water during photolysis using the three different lamps described in the text and shown in Figure S1. The rate constants were obtained from the slope of the plots.

Table 1. Photolysis Rate Constants (k_p) and Quantum Yields (ϕ) for NPM at pH ≈ 6 Solution Using Three Different Light Sources

experiments	photolysis wavelength (nm)	k_p (s^{-1})	ϕ
1	254	2.6×10^{-3}	0.25
2		1.5×10^{-3}	0.14
3		1.9×10^{-3}	0.18
4		2.1×10^{-3}	0.20
5		1.8×10^{-3}	0.17
6		1.9×10^{-3}	0.18
7		1.8×10^{-3}	0.17
average (±2σ)		$\mathbf{(1.9 \pm 0.7) \times 10^{-3}}$	**0.18 ± 0.07**
1	313	1.3×10^{-4}	0.08
2		1.6×10^{-4}	0.10
3		1.6×10^{-4}	0.10
4		1.4×10^{-4}	0.09
5		1.5×10^{-4}	0.09
6		1.6×10^{-4}	0.10
7		1.6×10^{-4}	0.10
average (±2σ)		$\mathbf{(1.5 \pm 0.3) \times 10^{-4}}$	$\mathbf{(9.4 \pm 1.6) \times 10^{-2}}$
1	350	5.5×10^{-5}	5.1×10^{-2}
2		4.9×10^{-5}	4.6×10^{-2}
3		5.9×10^{-5}	5.5×10^{-2}
4		6.4×10^{-5}	6.0×10^{-2}
5		5.2×10^{-5}	4.8×10^{-2}
average (±2σ)		$\mathbf{(5.6 \pm 1.2) \times 10^{-5}}$	$\mathbf{(5.2 \pm 1.1) \times 10^{-2}}$

Table 1 summarizes the measured quantum yields for each of the three photolysis lamps. These quantum yields are more than an order of magnitude larger than those measured in thin solid films.[44] This is not surprising because the solid provides a rigid cage structure around the fragments as they separate, enhancing their recombination. The cage effect in liquids is much less effective in holding the fragments together, giving a more efficient net dissociation.

Todey et al.[45] and González-Mariño et al.[46] recently reported quantum yields and products for photolysis of NPM in purified or river water. Table 2 compares their results to those in the

DOI: 10.1021/acsearthspacechem.9b00179
ACS Earth Space Chem. 2019, 3, 2063−2075

Table 2. Yields (ϕ) for NPM in Water Using Different Light Sources

light source	water source	ϕ[a]	reference
254 nm lamp	Milli-Q	0.18 ± 0.07	this work
313 nm lamp	Milli-Q	0.094 ± 0.016	this work
350 nm lamp	Milli-Q	0.052 ± 0.011	this work
254 nm lamp	Milli-Q	0.0495 ± 0.002[b]	González-Mariño et al.[46]
	river water	0.0385 ± 0.001[b]	González-Mariño et al.[46]
natural sunlight	Milli-Q	0.0534 ± 0.003[b]	González-Mariño et al.[46]
	river water	0.0442 ± 0.002[b]	González-Mariño et al.[46]
solar simulator	Milli-Q	0.025 ± 0.001	Todey et al.[45]
	Mississippi River water	0.023 ± 0.001	Todey et al.[45]
natural sunlight	Milli-Q	0.025 ± 0.001	Todey et al.[45]
	Mississippi River water	0.024 ± 0.001	Todey et al.[45]

[a]Errors are $\pm 2\sigma$. [b]Errors based on those cited for the photolysis rate constants.

current study. The values from Todey et al.[45] for purified water using a solar simulator or natural sunlight are about a factor of four and two smaller than our measured values using the 313 and 350 nm lamps, respectively. The main differences between their experiments and ours are the spectral distributions of the light sources and the actinometers that were used. The intensity of solar simulators and natural sunlight rise rapidly with wavelength above 300 nm.[43] Our measurements over three wavelength ranges in water at pH ~ 6 show that the quantum yields decrease from 0.18 at 254 nm, 0.094 for broadband radiation centered at 313 nm, to 0.052 for broadband centered at 350 nm. This trend of decreasing quantum yield with increasing wavelength is consistent with photolysis at longer wavelengths playing a larger role in their experiments. The quantum yield in pure water under natural sunlight reported by González-Mariño et al.[46] is in excellent agreement with our value for radiation centered at 350 nm, but their value for 254 nm is about a factor of three smaller than that measured here. Both Todey et al.[45] and González-Mariño et al.[46] identified a product with exact mass 227.08254, and González-Mariño et al.[46] also reported a number of other products.

Photolysis products were also measured here using ESI−MS. Figure 9 shows the ESI−MS before and after photolysis at 350 nm for 180 min. Major product peaks at m/z 212 and 258 are observed. These were attributed to $[M + H]^+$ peaks, and thus the products must have masses 211 and 257 Da, respectively. Figure 10 shows the MS−MS of each of these product peaks and Figure 11 shows the UV−vis absorption spectra of each product as they elute from the HPLC column. The lack of absorption above 275 nm suggests little or no contribution from a nitroenamine group.

The product with mass 211 Da is identified as **A**:

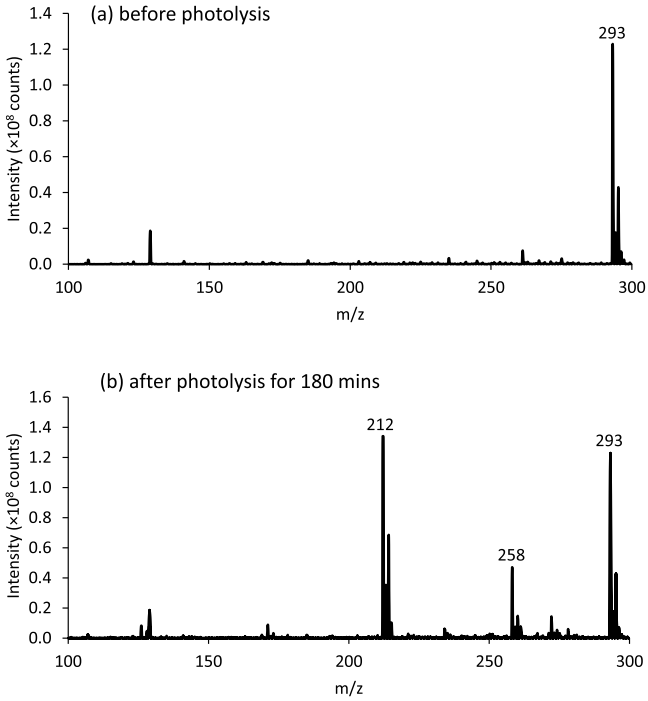

Figure 9. ESI−MS of NPM (a) before photolysis and (b) after photolysis for 180 min using the 350 nm lamp.

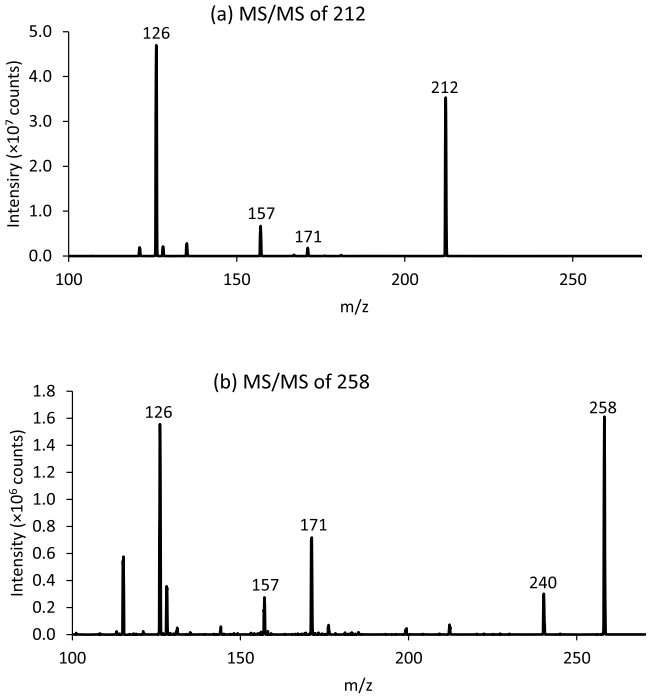

Figure 10. ESI−MS/MS with a collision energy of 15 eV of NPM photolysis products at (a) m/z 212 and (b) 258 ($[M + H]^+$), respectively, using the 350 nm lamp.

DOI: 10.1021/acsearthspacechem.9b00179
ACS Earth Space Chem. 2019, 3, 2063−2075

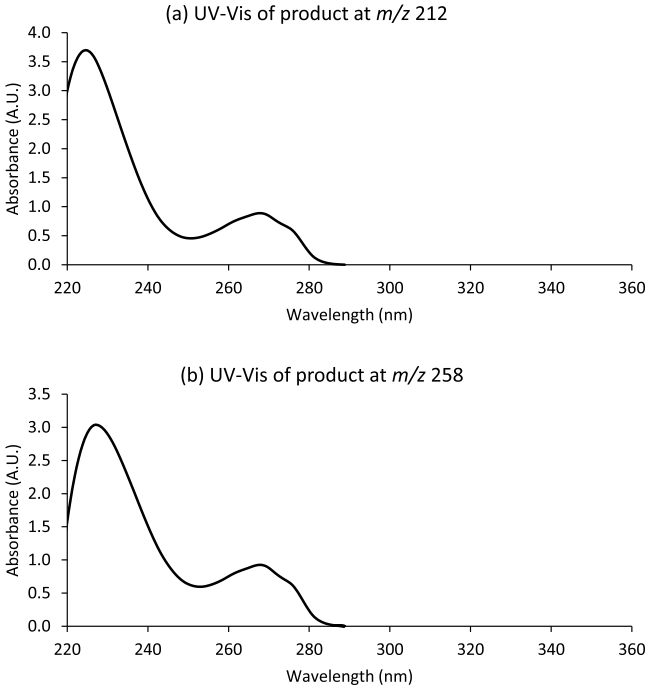

Figure 11. UV−vis spectra of products of NPM photolysis at (a) m/z 212 and (b) 258 ($[M + H]^+$), respectively, from HPLC−PDA.

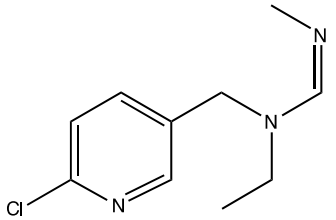

Exact Mass: 211.09 **A**

The product with mass 257 Da is identified as **B**:

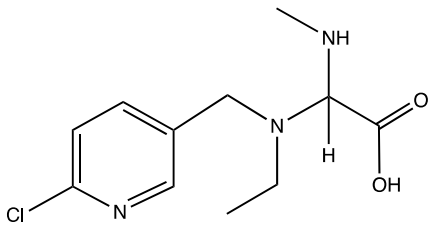

Exact Mass: 257.09 **B**

Product **A** was a major product in the photolysis of solid thin films of NPM.[44] It also agrees with a previous identification of this species in water[36,45,46] with a major MS−MS fragment at 126 and other fragments at 157 and 171 (Figure 10a). Noestheden et al.[36] also reported a product at m/z 257, but did not propose a structure. Todey et al.[45] reported a product at m/z 257 in the hydrolysis of NPM, with a different MS/MS pattern from ours. The fragment at m/z 240 (Figure 10b) corresponding to loss of water from m/z 258 as expected for a carboxylic acid, and the lack of an absorption band above 300 nm (Figure 11), support the structure of a carboxylic acid, product **B** proposed here. Figure 12 shows a potential formation mechanism for this product.

Using an average quantum yield of $\phi = 0.07 \pm 0.03$ from the 313 and 350 nm photolysis experiments, the lifetime of NPM ($\tau = 1/k_p$) in water at a solar zenith angle of 35°, typical of conditions on April 1 at 40° N latitude, is estimated to be only 5 min. This can be compared to 36 min for photolysis of solid NPM under the same conditions, illustrating the importance of the matrix in determining environmental fates of pesticides. Because of their short photolysis time to form products A and B, and their lack of absorption at $\lambda > 300$ nm (Figure 11), these may be expected to be found in aqueous environments where NPM is used.

CONCLUDING REMARKS

This work illustrates the importance of the medium in which an environmental contaminant is found in determining its properties, lifetimes, and fates. It also illustrates the critical role of theory in understanding at a molecular-level changes in the chemistry, absorption spectra, and photochemistry that occur in different media, and in revealing unexpected processes such as transfer of the proton from an amine nitrogen to the $-NO_2$ group.

ASSOCIATED CONTENT

Supporting Information

The Supporting Information is available free of charge on the ACS Publications website at DOI: 10.1021/acsearthspacechem.9b00179.

Emission spectra of photolysis lamps and transmission of glass filter, photolysis rate of ONB (k_{ONB}) and absolute light intensities, parameters for UPLC−ESI−MS/MS, HPLC−MS, and ESI−MS/MS, excel Solver aid in determining composition spectra, calculated vertical excitation energies and orbitals of neutral and protonated NPM, and solvation dynamics (PDF)

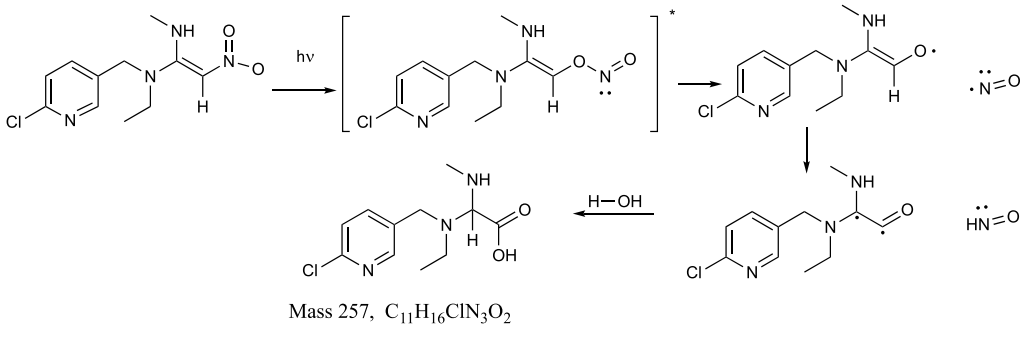

Figure 12. Proposed mechanism for formation of the photolysis product at m/z 258 (mass 257).

DOI: 10.1021/acsearthspacechem.9b00179
ACS Earth Space Chem. 2019, 3, 2063−2075

AUTHOR INFORMATION

Corresponding Authors

*E-mail: bgerber@uci.edu (R.B.G.) for theory.
*E-mail: bjfinlay@uci.edu (B.J.F.-P.) for experiment.

ORCID

Barbara J. Finlayson-Pitts: 0000-0003-4650-168X

Author Contributions

§Equal first co-authors.

Notes

The authors declare no competing financial interest.

ACKNOWLEDGMENTS

We are grateful to the National Science Foundation for support of this work (grant #1404233) and the NSF Major Research Instrumentation (MRI) program (grant #1337080). We also thank Felix Grun and Veronique Perraud for assistance with the UPLC−MS experiments.

REFERENCES

(1) Elbert, A.; Haas, M.; Springer, B.; Thielert, W.; Nauen, R. Applied aspects of neonicotinoid uses in crop protection. *Pest Manag. Sci.* **2008**, *64*, 1099−1105.

(2) Bonmatin, J.-M.; Giorio, C.; Girolami, V.; Goulson, D.; Kreutzweiser, D. P.; Krupke, C.; Liess, M.; Long, E.; Marzaro, M.; Mitchell, E. A. D.; Noome, D. A.; Simon-Delso, N.; Tapparo, A. Environmental fate and exposure; neonicotinoids and fipronil. *Environ. Sci. Pollut. Res.* **2015**, *22*, 35−67.

(3) Furlan, L.; Pozzebon, A.; Duso, C.; Simon-Delso, N.; Sánchez-Bayo, F.; Marchand, P. A.; Codato, F.; Bijleveld van Lexmond, M.; Bonmatin, J.-M. An update of the Worldwide Integrated Assessment (WIA) on systemic insecticides. Part 3: alternatives to systemic insecticides. *Environ. Sci. Pollut. Res.* **2018**, 1−23.

(4) Giorio, C.; Safer, A.; Sánchez-Bayo, F.; Tapparo, A.; Lentola, A.; Girolami, V.; van Lexmond, M. B.; Bonmatin, J.-M. An update of the Worldwide Integrated Assessment (WIA) on systemic insecticides. Part 1: New molecules, metabolism, fate, and transport. *Environ. Sci. Pollut. Res.* **2017**, DOI: 10.1007/s11356-017-0394-3.

(5) Pisa, L.; Goulson, D.; Yang, E.-C.; Gibbons, D.; Sánchez-Bayo, F.; Mitchell, E.; Aebi, A.; van der Sluijs, J.; MacQuarrie, C. J. K.; Giorio, C.; Long, E. Y.; McField, M.; Bijleveld van Lexmond, M.; Bonmatin, J.-M. An update of the Worldwide Integrated Assessment (WIA) on systemic insecticides. Part 2: Impacts on organisms and ecosystems. *Environ. Sci. Pollut. Res.* **2017**, DOI: 10.1007/s11356-017-0341-3.

(6) Simon-Delso, N.; Amaral-Rogers, V.; Belzunces, L. P.; Bonmatin, J. M.; Chagnon, M.; Downs, C.; Furlan, L.; Gibbons, D. W.; Giorio, C.; Girolami, V.; Goulson, D.; Kreutzweiser, D. P.; Krupke, C. H.; Liess, M.; Long, E.; McField, M.; Mineau, P.; Mitchell, E. A. D.; Morrissey, C. A.; Noome, D. A.; Pisa, L.; Settele, J.; Stark, J. D.; Tapparo, A.; Van Dyck, H.; Van Praagh, J.; Van der Sluijs, J. P.; Whitehorn, P. R.; Wiemers, M. Systemic insecticides (neonicotinoids and fipronil): trends, uses, mode of action and metabolites. *Environ. Sci. Pollut. Res.* **2015**, *22*, 5−34.

(7) van Lexmond, M. B.; Bonmatin, J.-M.; Goulson, D.; Noome, D. A. Worldwide integrated assessment on systemic pesticides. *Environ. Sci. Pollut. Res.* **2015**, *22*, 1−4.

(8) Matsuda, K.; Buckingham, S. D.; Kleier, D.; Rauh, J. J.; Grauso, M.; Sattelle, D. B. Neonicotinoids: insecticides acting on insect nicotinic acetylcholine receptors. *Trends Pharmacol. Sci.* **2001**, *22*, 573−580.

(9) Alkassab, A. T.; Kirchner, W. H. Sublethal exposure to neonicotinoids and related side effects on insect pollinators: honeybees, bumblebees, and solitary bees. *J. Plant Dis. Protect.* **2017**, *124*, 1−30.

(10) Benuszak, J.; Laurent, M.; Chauzat, M.-P. The exposure of honey bees (Apis mellifera ; Hymenoptera: Apidae) to pesticides: Room for improvement in research. *Sci. Total Environ.* **2017**, *587*−*588*, 423−438.

(11) Botías, C.; David, A.; Horwood, J.; Abdul-Sada, A.; Nicholls, E.; Hill, E.; Goulson, D. Neonicotinoid residues in wildflowers, a potential route of chronic exposure for bees. *Environ. Sci. Technol.* **2015**, *49*, 12731−12740.

(12) Botías, C.; David, A.; Horwood, J.; Abdul-Sada, A.; Nicholls, E.; Hill, E.; Goulson, D. Response to Comment on "Neonicotinoid Residues in Wildflowers, A Potential Route of Chronic Exposure for Bees". *Environ. Sci. Technol.* **2016**, *50*, 1630−1631.

(13) Decourtye, A.; Devillers, J. Ecotoxicity of neonicotinoid insecticides to bees. In *Insect Nicotinic Acetylcholine Receptors*; Thany, S. H., Ed.; Springer-Verlag: New York, 2010; Vol. *683*, pp 85−95.

(14) Di Prisco, G.; Cavaliere, V.; Annoscia, D.; Varricchio, P.; Caprio, E.; Nazzi, F.; Gargiulo, G.; Pennacchio, F. Neonicotinoid clothianidin adversely affects insect immunity and promotes replication of a viral pathogen in honey bees. *PNAS* **2013**, *110*, 18466−18471.

(15) Doublet, V.; Labarussias, M.; de Miranda, J. R.; Moritz, R. F. A.; Paxton, R. J. Bees under stress: sublethal doses of a neonicotinoid pesticide and pathogens interact to elevate honey bee mortality across the life cycle. *Environ. Microbiol.* **2015**, *17*, 969−983.

(16) Kessler, S. C.; Tiedeken, E. J.; Simcock, K. L.; Derveau, S.; Mitchell, J.; Softley, S.; Radcliffe, A.; Stout, J. C.; Wright, G. A. Bees prefer foods containing neonicotinoid pesticides. *Nature* **2015**, *521*, 74−76.

(17) Klein, S.; Cabirol, A.; Devaud, J.-M.; Barron, A. B.; Lihoreau, M. Why bees are so vulnerable to environmental stressors. *Trends Ecol. Evol.* **2017**, *32*, 268−278.

(18) LaLone, C. A.; Villeneuve, D. L.; Wu-Smart, J.; Milsk, R. Y.; Sappington, K.; Garber, K. V.; Housenger, J.; Ankley, G. T. Weight of evidence evaluation of a network of adverse outcome pathways linking activation of the nicotinic acetylcholine receptor in honey bees to colony death. *Sci. Total Environ.* **2017**, *584*−*585*, 751−775.

(19) Mommaerts, V.; Reynders, S.; Boulet, J.; Besard, L.; Sterk, G.; Smagghe, G. Risk assessment for side-effects of neonicotinoids against bumblebees with and without impairing foraging behavior. *Ecotoxicology* **2010**, *19*, 207−215.

(20) Raine, N. E.; Gill, R. J. Tasteless pesticides affect bees in the field. *Nature* **2015**, *521*, 38−39.

(21) Rundlöf, M.; Andersson, G. K. S.; Bommarco, R.; Fries, I.; Hederström, V.; Herbertsson, L.; Jonsson, O.; Klatt, B. K.; Pedersen, T. R.; Yourstone, J.; Smith, H. G. Seed coating with a neonicotinoid insecticide negatively affects wild bees. *Nature* **2015**, *521*, 77−80.

(22) Solomon, K. R.; Stephenson, G. L. Quantitative weight of evidence assessment of higher-tier studies on the toxicity and risks of neonicotinoid insecticides in honeybees 1: Methods. *J. Toxicol. Environ. Health-B-Crit. Rev.* **2017**, *20*, 316−329.

(23) Solomon, K. R.; Stephenson, G. L. Quantitative weight of evidence assessment of higher tier studies on the toxicity and risks of neonicotinoids in honeybees. 3. Clothianidin. *J. Toxicol. Environ. Health-B-Crit. Rev.* **2017**, *20*, 346−364.

(24) Stanley, D. A.; Garratt, M. P. D.; Wickens, J. B.; Wickens, V. J.; Potts, S. G.; Raine, N. E. Neonicotinoid pesticide exposure impairs crop pollination services provided by bumblebees. *Nature* **2015**, *528*, 548−550.

(25) Stephenson, G. L.; Solomon, K. R. Quantitative weight of evidence assessment of higher-tier studies on the toxicity and risks of neonicotinoids in honeybees. 2. Imidacloprid. *J. Toxicol. Environ. Health-B-Crit. Rev.* **2017**, *20*, 330−345.

(26) Stephenson, G. L.; Solomon, K. R. Quantitative weight of evidence assessment of higher tier studies on the toxicity and risks of neonicotinoids in honeybees. 4. Thiamethoxam. *J. Toxicol. Environ. Health-B-Crit. Rev.* **2017**, *20*, 365−382.

(27) European Union, *Document L:2018:132:TOC, Official Journal of the European Union*, L 132, 61, May 30, 2018.

(28) Pest Management Regulatory Agency, Government of Canada, *Proposed Re-evaluation Decision PRVD2018-12, Imidacloprid and its Associated End-Use Products: Pollinator Re-evaluation*: Ottawa, Canada, May 31, 2018.

(29) Zhang, Z.; Zhang, X.; Wang, Y.; Zhao, Y.; Lin, J.; Liu, F.; Mu, W. Nitenpyram, dinotefuran, and thiamethoxam used as seed treatments act as efficient controls against Aphis gossypii via high residues in cotton leaves. *J. Agric. Food Chem.* **2016**, *64*, 9276−9285.

DOI: 10.1021/acsearthspacechem.9b00179
ACS Earth Space Chem. 2019, 3, 2063−2075

(30) Beck, W.; Saunders, M.; Schunack, B.; Pfister, K. Flea control in wild, rescued hedgehogs - A therapeutic approach with nitenpyram (Capstar (R)). *Der Praktische Tierarz* **2005**, *86*, 798−802.
(31) Chatellier, K. Nitenpyram. *Compend Contin. Educ. Vet.* **2001**, *23*, 748−749.
(32) McCoy, C.; Broce, A. B.; Dryden, M. W. Flea blood feeding patterns in cats treated with oral nitenpyram and the topical insecticides imidacloprid, fipronil and selamectin. *Vet. Parasitol.* **2008**, *156*, 293−301.
(33) Rust, M. K.; Waggoner, M. M.; Hinkle, N. C.; Stansfield, D.; Barnett, S. Efficacy and longevity of nitenpyram against adult cat fleas (Siphonaptera: Pulicidae). *J. Med. Entomol.* **2003**, *40*, 678−681.
(34) Schenker, R.; Tinembart, O.; Humbert-Droz, E.; Cavaliero, T.; Yerly, B. Comparative speed of kill between nitenpyram, fipronil, imidacloprid, selamectin and cythioate against adult Ctenocephalides felis (Bouché) on cats and dogs. *Vet. Parasitol.* **2003**, *112*, 249−254.
(35) Zhang, Z.; Wang, Y.; Zhao, Y. H.; Li, B. X.; Lin, J.; Zhang, X. F.; Liu, F.; Mu, W. Nitenpyram seed treatment effectively controls against the mirid bug Apolygus lucorum in cotton seedlings. *Sci. Rep.* **2017**, *7*, 8572.
(36) Noestheden, M.; Roberts, S.; Hao, C. Nitenpyram degradation in finished drinking water. *Rapid Commun. Mass Spectrom.* **2016**, *30*, 1653−1661.
(37) Obana, H.; Okihashi, M.; Akutsu, K.; Kitagawa, Y.; Hori, S. Determination of acetamiprid, imidacloprid, and nitenpyram residues in vegetables and fruits by high-performance liquid chromatography with diode-array detection. *J. Agric. Food Chem.* **2002**, *50*, 4464−4467.
(38) Tsumura, Y.; Nakamura, Y.; Tonogai, Y.; Kakimoto, Y.; Tanaka, Y.; Shibata, T. Determination of neonicotinoid pesticide nitenpyram and its metabolites in agricultural products. *J. Food Hygien. Soc. Japan* **1998**, *39*, 127−134.
(39) Yoshida, T.; Murakawa, H.; Toda, K. Determination of nitenpyram and its metabolites in agricultural products by using hydrophilic interaction liquid chromatography-tandem mass spectrometry. *J. Pest. Sci.* **2013**, *38*, 27−32.
(40) Morrissey, C. A.; Mineau, P.; Devries, J. H.; Sanchez-Bayo, F.; Liess, M.; Cavallaro, M. C.; Liber, K. Neonicotinoid contamination of global surface waters and associated risk to aquatic invertebrates: A review. *Environ. Int.* **2015**, *74*, 291−303.
(41) Osaka, A.; Ueyama, J.; Kondo, T.; Nomura, H.; Sugiura, Y.; Saito, I.; Nakane, K.; Takaishi, A.; Ogi, H.; Wakusawa, S.; Ito, Y.; Kamijima, M. Exposure characterization of three major insecticide lines in urine of young children in Japan-neonicotinoids, organophosphates, and pyrethroids. *Environ. Res.* **2016**, *147*, 89−96.
(42) Amelin, V. G.; Bol'shakov, D. S.; Andoralov, A. M. Determination of neonicotinoid insecticides in natural waters by high-resolution time-of-flight mass spectrometry with direct electrospray ionization of samples. *J. Anal. Chem.* **2017**, *72*, 178−182.
(43) Finlayson-Pitts, B. J.; Pitts, J. N. *Chemistry of the Upper and Lower Atmosphere: Theory, Experiments, and Applications*; Academic Press: San Diego, 2000; p 969.
(44) Aregahegn, K. Z.; Ezell, M. J.; Finlayson-Pitts, B. J. Photochemistry of solid films of the neonicotinoid nitenpyram. *Environ. Sci. Technol.* **2018**, *52*, 2760−2767.
(45) Todey, S. A.; Fallon, A. M.; Arnold, W. A. Neonicotinoid insecticide hydrolysis and photolysis: Rates and residual toxicity. *Environ. Toxicol. Chem.* **2018**, *37*, 2797−2809.
(46) González-Mariño, I.; Rodríguez, I.; Rojo, L.; Cela, R. Photodegradation of nitenpyram under UV and solar radiation: Kinetics, transformation products identification and toxicity prediction. *Sci. Total Environ.* **2018**, *644*, 995−1005.
(47) Cholerton, T. J.; Hunt, J. H.; Klinkert, G.; Martin-Smith, M. Spectroscopic studies on ranitidine-Its structure and the influence of temperature and pH. *J. Chem. Soc. Perkin Trans. 2* **1984**, 1761−1766.
(48) De Armas, H. N.; Peeters, O. M.; Blaton, N.; Van Gyseghem, E.; Martens, J.; Van Haele, G.; Van den Mooter, G. Solid state characterization and crystal structure from X-Ray powder diffraction of two polymorphic forms of ranitidine base. *J. Pharm. Sci.* **2009**, *98*, 146−158.
(49) Haywood, P. A.; Martin-Smith, M.; Cholerton, T. J.; Evans, M. B. Isolation and identification of the hydrolytic degradation products of ranitidine hydrochloride. *J. Chem. Soc. Perkin Trans. 1* **1987**, 951−954.
(50) Agatonovic-Kustrin, S.; Rades, T.; Wu, V.; Saville, D.; Tucker, I. G. Determination of polymorphic forms of ranitidine-HCl by DRIFTS and XRPD. *J. Pharm. Biomed. Anal.* **2001**, *25*, 741−750.
(51) Dumanović, D.; Juranić, I.; Dzeletovic, D.; Vasic, V. M.; Jovanovic, J. Protolytic constants of nizatidine, ranitidine and N,N'-dimethyl-2-nitro-1,1-ethenediamine; spectrophotometric and theoretical investigation. *J. Pharm. Biomed. Anal.* **1997**, *15*, 1667−1678.
(52) Ishida, T.; In, Y.; Inoue, M. Structure of ranitidine hydrochloride. *Acta Crystall. C.-Cryst. Struct. Commun.* **1990**, *46*, 1893−1896.
(53) Mirmehrabi, M.; Rohani, S.; Murthy, K. S. K.; Radatus, B. Solubility, dissolution rate and phase transition studies of ranitidine hydrochloride tautomeric forms. *Int. J. Pharm.* **2004**, *282*, 73−85.
(54) Mirmehrabi, M.; Rohani, S.; Murthy, K. S. K.; Radatus, B. Characterization of tautomeric forms of ranitidine hydrochloride: thermal analysis, solid-state NMR, X-ray. *J. Cryst. Growth* **2004**, *260*, 517−526.
(55) Dhaked, D. K.; Bharatam, P. V. Nitro reversible arrow aci-nitro tautomerism and E/Z isomeric preferences of nitroethenediamine derivatives: a quantum chemical study. *RSC Adv.* **2013**, *3*, 25268−25277.
(56) Kleier, D.; Holden, I.; Casida, J. E.; Ruzo, L. O. Novel photoreactions of an insecticidal nitromethylene heterocycle. *J. Agric. Food Chem.* **1985**, *33*, 998−1000.
(57) Kagabu, S.; Medej, S. Stability Comparison of Imidacloprid and Related Compounds under Simulated Sunlight, Hydrolysis Conditions, and to Oxygen. *Biosci. Biotech. Biochem.* **1995**, *59*, 980−985.
(58) Galbavy, E. S.; Ram, K.; Anastasio, C. 2-Nitrobenzaldehyde as a chemical actinometer for solution and ice photochemistry. *J. Photochem. Photobiol A-Chemistry* **2010**, *209*, 186−192.
(59) Xu, L.-Z.; Yang, Z.; Yi, X.; An, G.-W. (E)-N-(6-Chloro-3-pyridylmethyl)-N-ethyl-N′-methyl-2-nitroethylene-1,1-diamine. *Acta Crystallogr. E* **2008**, *64*, O1074.
(60) Wavefunction Inc. *Spartan 14*, Irvine, CA.
(61) Weber, W.; Thiel, W. Orthogonalization corrections for semiempirical methods. *Theor. Chem. Acc.* **2000**, *103*, 495−506.
(62) Thiel, W. *MNDO Program*; Max-Planck-Institut fur Kohlenforschung: Mulheim: Germany, 2017.
(63) Aregahegn, K. Z.; Shemesh, D.; Gerber, R. B.; Finlayson-Pitts, B. J. Photochemistry of thin solid films of the neonicotinoid imidacloprid on surfaces. *Environ. Sci. Technol.* **2017**, *51*, 2660−2668.
(64) Weigend, F.; Häser, M. RI-MP2: first derivatives and global consistency. *Theor. Chem. Acc.* **1997**, *97*, 331−340.
(65) Ahlrichs, R.; Bär, M.; Häser, M.; Horn, H.; Kölmel, C. Electronic structure calculations on workstation computers: The program system turbomole. *Chem. Phys. Lett.* **1989**, *162*, 165−169.
(66) Dunning, T. H. Gaussian basis sets for use in correlated molecular calculations. I. The atoms boron through neon and hydrogen. *J. Chem. Phys.* **1989**, *90*, 1007−1023.
(67) Schirmer, J. Beyond the random-phase approximation: A new approximation scheme for the polarization propagator. *Phys. Rev. A* **1982**, *26*, 2395−2416.
(68) Epstein, S. A.; Shemesh, D.; Tran, V. T.; Nizkorodov, S. A.; Gerber, R. B. Absorption spectra and photolysis of methyl peroxide in liquid and frozen water. *J. Phys. Chem. A* **2012**, *116*, 6068−6077.
(69) Romonosky, D. E.; Nguyen, L. Q.; Shemesh, D.; Nguyen, T. B.; Epstein, S. A.; Martin, D. B. C.; Vanderwal, C. D.; Gerber, R. B.; Nizkorodov, S. A. Absorption spectra and aqueous photochemistry of β-hydroxyalkyl nitrates of atmospheric interest. *Mol. Phys.* **2015**, *113*, 2179−2190.
(70) Shemesh, D.; Gerber, R. B. Molecular dynamics of photoinduced reactions of acrylic acid: Products, mechanisms, and comparison with experiment. *J. Phys. Chem. Lett.* **2018**, *9*, 527−533.
(71) Shemesh, D.; Salomon, R.; Kim, S. H.; Tyndall, G. S.; Nizkorodov, S. A.; Gerber, R. B. Adjacent keto and enol groups in photochemistry of a cyclic molecule: Products, mechanisms and dynamics. *Chem. Phys.* **2018**, *515*, 177−186.

DOI: 10.1021/acsearthspacechem.9b00179
ACS Earth Space Chem. 2019, 3, 2063−2075

(72) Cook, A. G. *Enamines. Synthesis, Structure and Reactions*; Marcel Dekker: New York, 1988; p 717.
(73) Catalán, J.; Garcio Blanco, F. Acidity and basicity of enamines. In *The Chemistry of Enamines*; Rappoport, Z., Ed.; John Wiley & Sond: Chichester, 1994; Vol. *1*, pp 695−726.
(74) Williams, R.; Jencks, W. P.; Westheimer, F. H. pKa data compiled by R. Williams. Available online: https://www.chem.wisc.edu/areas/reich/pkatable/pKa_compilation-1-Williams.pdf (accessed on Dec 22, 2018).
(75) Cook, A. G.; Absi, M. L.; Bowden, V. K. Basicity of some mono- and bicyclic enamines and tricyclenamines. *J. Org. Chem.* **1995**, *60*, 3169−3171.
(76) Socrates, G. *Infrared and Raman Characteristic Group Frequencies*, 3rd ed.; Wiley, 2004.

DOI: 10.1021/acsearthspacechem.9b00179
ACS Earth Space Chem. 2019, 3, 2063−2075